


Article

Multiple Fano Resonances in Dynamic Resonant Tunneling Processes

Gilad Zangwill * and Er'el Granot * 

Department of Electrical and Electronics Engineering, Ariel Photonic Center, Ariel University, Ariel 40700, Israel
* Correspondence: gzangwill@gmail.com (G.Z.); erel@ariel.ac.il (E.G.)

Abstract: The existence of Fano resonances in dynamic resonant tunneling (RT) systems has been investigated. Fano resonances are characterized by the appearance of a 100% reflection coefficient in proximity to a high transmission coefficient. For a Fano resonance to appear, a bound state must exist. On the other hand, a resonant tunneling process is characterized by a high transmission and the existence of a quasi-bound state (QBS) instead of a bound one. It has been shown that, by narrowing the width of the barrier, the resonance energy of the QBS gradually decreases and eventually turns into a bound state. Consequently, in a dynamic RT process, there are two scenarios: either a bound state exists, in which case, Fano resonances exist for any barrier width, or a QBS exists, and the barrier should be narrow enough for the Fano resonance to appear. In both cases, the incoming particle's frequency must be lower than the oscillating well's frequency. In this work, these resonances are investigated in detail, and both exactly numerically and approximated analytical expressions are derived for both the weak and strong oscillating amplitude regimes. One of the conclusions is that, when the oscillating frequency is low enough, multiple Fano resonances can appear by varying the barrier's width. Since these resonances are very sharp and zero transmission can easily be detected, this property can be used as a very accurate method for measuring the barrier's width, even when the particle's de-Broglie wavelength is much larger than the barrier's width.

Keywords: resonant tunneling; quantum dynamics; dynamic resonant tunneling; suppression of tunneling; coherent destruction of tunneling; total reflection; Fano resonance; quasi-bound state



Citation: Zangwill, G.; Granot, E. Multiple Fano Resonances in Dynamic Resonant Tunneling Processes. *Appl. Sci.* **2023**, *13*, 6767. <https://doi.org/10.3390/app13116767>

Received: 20 April 2023
Revised: 23 May 2023
Accepted: 31 May 2023
Published: 2 June 2023



Copyright: © 2023 by the authors. Licensee MDPI, Basel, Switzerland. This article is an open access article distributed under the terms and conditions of the Creative Commons Attribution (CC BY) license (<https://creativecommons.org/licenses/by/4.0/>).

1. Introduction

Tunneling and Resonant Tunneling are quantum processes that are extremely sensitive to a particle's energy. Consequently, when a system incorporates dynamic structures, its behavior can become much more complex. In general, perturbations, which are introduced into the system, usually tend to increase the tunneling current. This behavior manifests in activation [1–9] and the elevator effect [8,9]. However, in some cases, for some specific energies, the tunneling current can be substantially suppressed [10–20]. In particular, it has been shown that 100% reflection occurs in certain cases. This conduct is related to Fano resonances [21–28].

Recently, a different presentation of current suppression and activation was demonstrated. It was shown that, when a particle penetrates an opaque barrier via a varying well, the process can be regarded as if the particle is trapped in a Quasi-Bound Super State (QBSS) [14], in a similar fashion to a Resonant Tunneling process, in which the particle is trapped in a Quasi-Bound State [29–32]. The difference between these two scenarios is that the QBSS consists of multiple sub-quasi-states. Consequently, when an incoming particle's energy matches a high-amplitude spectral component of the QBSS, a high transmission occurs, and similarly, when no match occurs, the current is suppressed. It was noted that, at these energies, a destructive interference occurs in the well, which prevents particles from dwelling in this well, therefore preventing a high transmission. In these cases, the current decreases drastically; however, it is not necessarily reduced to zero, i.e., it does not

necessarily show Fano behavior. In fact, the same system may exhibit both behaviors for different energies in different cases.

A Fano resonance occurs due to interference between a bound state and a continuum state. It is, therefore, not straightforwardly clear how a Fano resonance appears in a system that exhibits RT behavior. After all, an RT requires a quasi-bound state and not a bound one.

The width of the barrier affects the resonance energy; however, in most research, this phenomenon has received little attention, mainly due to two reasons: first, in a resonant tunneling process, the barrier is usually opaque, and therefore its specific width has a negligible effect on the resonance energy (which predominantly depends on the shape of the potential well), and second, by narrowing the barrier, the resonance’s spectral width increases (i.e., the particle’s dwelling time in the well decreases); therefore, the resonance nature of the process fades away. Therefore, when the barrier is too narrow, it is fruitless to analyze the process as an RT one. This is indeed true in the stationary case, but in the dynamic case, the situation is much more complicated. Some of these effects have been observed in recent research [21,27].

We will show, in the following sections, that, by narrowing the barrier, not only does the resonance energy decrease drastically, but it can also be negative. Therefore, the barrier’s width shrinkage can turn a resonance state into a bound one. Clearly, in a stationary scattering case, the bound state cannot be reached; however, in a dynamic case, the quasi-bound state generates a Fano resonance, which causes 100% reflection. Moreover, since the particle can lose/gain any number of energy quanta, then, if the oscillating frequency is low enough, by changing the barrier’s width, multiple Fano resonances can occur for the same incoming particle’s energy.

2. The Transition from a Resonant State to a Bound State and Its Dependence on the Barrier’s Width

In a stationary Resonant Tunneling process, particles tunnel through an opaque barrier via a quasi-bound state (QBS). A QBS can be formed by locating a potential well within a barrier, as described by the following stationary Schrödinger equation:

$$\left[-\frac{\partial^2}{\partial x^2} + U(x) - \Omega + \alpha\delta(x) \right] \psi(x) = 0 \tag{1}$$

where $U(x) = \begin{cases} U & -L < x < L \\ 0 & \text{else} \end{cases}$ is the potential barrier and the potential well is described by a delta function potential. Hereinafter, we use, for simplicity, but without a loss of generality, the units $\hbar = 1$ and $2m = 1$ for the Planck constant and the electron’s mass, respectively.

The system schematic is presented in Figure 1.

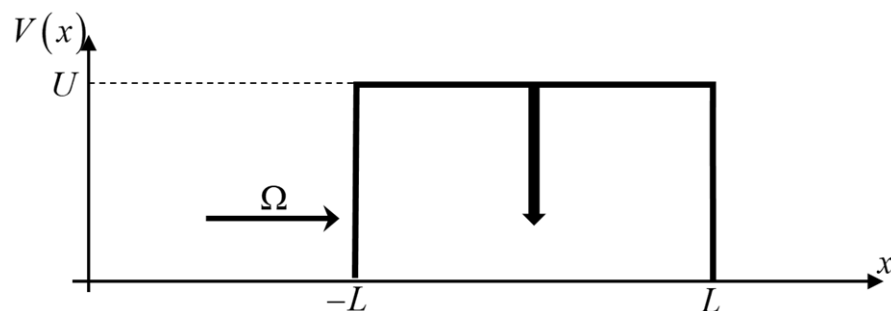


Figure 1. Particles with energy Ω propagate through a rectangular potential barrier with a delta function potential well at its center. The barrier height is U and its width is $2L$.

It should be noted that a delta function potential is an excellent approximation for a narrow well, as long as the width of the well is narrower than the De-Broglie wavelength of the QBS [32].

The solution of Equation (1) is:

$$\psi(x) = \psi_h(x) + \frac{\alpha\psi_h(0)}{1 - \alpha G_{\Omega}^+(0)} G_{\Omega}^+(x > L) \tag{2}$$

where $\psi_h(x)$ is the homogeneous solution (without the well) and $G_{\Omega}^+(x)$ is the outgoing Green function of Equation (1) without the well. For a rectangular barrier, the Green function at $x = 0$ is [11,33]:

$$G_{\Omega}^+(0) = -\frac{1}{2\rho} \coth\left(\rho L - i \arctan\left(\frac{k}{\rho}\right)\right) \tag{3}$$

where $k \equiv \sqrt{\Omega}$ and $\rho \equiv \sqrt{U - \Omega}$.

In the case of an extremely opaque barrier, i.e., $L\sqrt{U} \gg 1$, the Green function at $x = 0$ is approximately $G_{\Omega}^+(0) \cong -1/2\rho$ and the Resonance Energy of the Opaque Barrier (REOB) is simply:

$$\Omega_R(L \rightarrow \infty) \equiv U - \frac{\alpha^2}{4} \tag{4}$$

When the incoming particle’s energy is equal to this resonance energy, the particle will tunnel through the barrier via the QBS with a high probability. Equation (4) is derived for a completely opaque barrier. In general, the resonance energy is a function of the barrier’s parameters (potential height U and width L). In particular, the resonance energy decreases when the barrier becomes narrower.

The relation between the resonance energy and the barrier’s width can be derived from the denominator of Equation (2) (the real part determines the energy and the imaginary part determines its spectral width), i.e., the energy that solves $1 - \alpha G_{\Omega}^+(0) = 0$ is the resonance energy. In solving for $L(\Omega_R)$ to obtain a generic expression for the barrier’s width as a function of the resonance energy, we find:

$$L(\Omega_R) = -\frac{1}{\rho_R} \left(\operatorname{arctanh}\left[\frac{\alpha}{2\rho_R}\right] + \operatorname{arctanh}\left(-i\frac{k_R}{\rho_R}\right) \right) \tag{5}$$

where $k_R \equiv \sqrt{\Omega_R}$ and $\rho_R \equiv \sqrt{U - \Omega_R}$.

Equation (5) shows that, for $\Omega_R = U - \alpha^2/4$, the barrier’s width is infinite; however, for any $\Omega_R < U - \alpha^2/4$, there is a barrier with a certain width, which supports this resonance energy, and the lower the resonance energy, the narrower the barrier must be. In particular, at a certain width, the barrier’s resonance energy is zero:

$$L_0 \equiv L(\Omega_R = 0) = U^{-1/2} \operatorname{arctanh}\left(|\alpha|/2\sqrt{U}\right) \tag{6}$$

Below this value, i.e., for $L < L_0$, the resonance energy becomes negative and the resonance state turns into a bound state.

In Figure 2, the transmission probability (a contour presentation) is presented as a function of both the width of the barrier L and the particle’s energy Ω . Equation (5) is represented by a red dashed curve. As can be seen, the resonance energy presented by Equation (5) agrees with a high transmission coefficient.

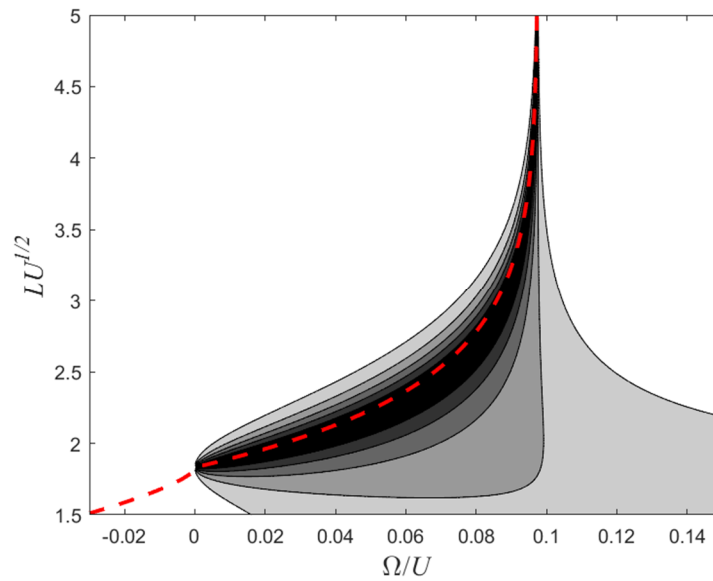


Figure 2. Contour plot of the transmission coefficient of the barrier as a function of both the particle's energy Ω and the barrier's width L (for the case $\alpha U^{-1/2} = -1.9$). The darker the color, the higher the transmission coefficient. The dashed red curve represents Equation (5). In the positive energy regime it represents a resonant state and in the negative energy regime it represents a bound state.

When the barrier gets narrower, the spectral width of the resonance gets wider and the center of the spectrum shifts to a lower energy. This behavior is seen in the black area in Figure 2. Eventually, for a width smaller than L_0 (Equation (6)), this energy becomes negative and the resonance state turns into a bound state. Therefore, although the well is elevated by the barrier's presence and despite the fact that only the width of the barrier has changed (and not its height), the resonance energy drastically decreases and can even be negative. Consequently, if the barrier is narrow enough, the resonant state becomes a bound state, despite the fact that the well's energy is lower than the barrier's height ($\alpha^2/4 < U$).

3. Total Reflection via Narrow Barriers

From the stationary problem above, we learn that barrier narrowing shifts the resonance to lower energies and even negative ones. Clearly, in this stationary scenario, it is not very useful, since there is no access to the bound state and the resonance states are too spectrally wide. However, when the well oscillates, the particle can lose oscillation quanta and be transferred, at least temporally, to the bound state. Consequently, a Fano resonance can be generated.

In the dynamic scenario, an oscillating component is added, and the Schrödinger equation reads:

$$-\frac{\partial^2}{\partial x^2}\psi + U(x)\psi + (\alpha + \beta \cos \omega t)\delta(x)\psi = i\frac{\partial \psi}{\partial t} \tag{7}$$

The dynamic system is illustrated in Figure 3.

The solution of Equation (7) can be written as a superposition of discrete energy expressions:

$$\psi(x, t) = \begin{cases} \varphi_0^+ \exp(-i\Omega_0 t) + \sum_{n=-\infty}^{\infty} r_n \varphi_n^- \exp(-i\Omega_n t) & x < 0 \\ \sum_{n=-\infty}^{\infty} t_n \varphi_n^+ \exp(-i\Omega_n t) & x > 0 \end{cases} \tag{8}$$

where φ_n^\pm are the homogeneous solutions of waves that propagate from left to right (φ_n^+) and from right to left (φ_n^-), i.e.,

$$\varphi_n^+ \rightarrow \tau_{\Omega_n} \exp[ik_n x - i\Omega_n t] \text{ (for } x \rightarrow \infty) \tag{9}$$

$$\varphi_n^- \rightarrow \tau_{\Omega_n} \exp[-ik_n x - i\Omega_n t] \text{ (for } x \rightarrow -\infty) \tag{10}$$

where $k_n = \sqrt{\Omega_n}$, $\Omega_n \equiv \Omega + n\omega$. $|\tau_{\Omega}|^2$ is the probability of penetrating the stationary barrier with energy Ω , and finally, r_n and t_n are the modes' coefficients. It is worth noting the difference between the coefficients of the modes, i.e., r_n and t_n , which need to be found, and the transmission coefficient of a single mode τ_{Ω_n} , which is obtained by solving the stationary case.

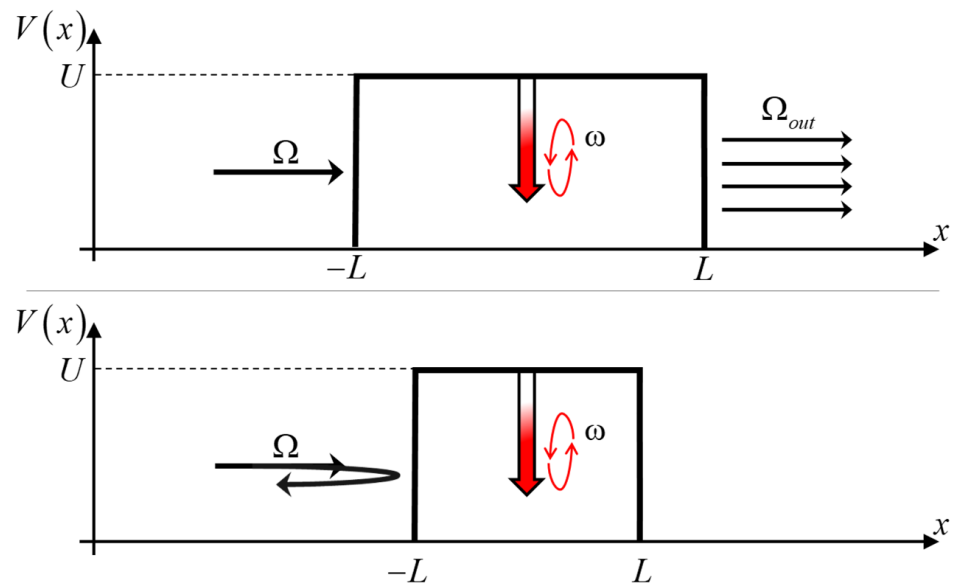


Figure 3. Incoming particles propagate through a potential barrier with an oscillating part at its center. **Upper panel:** the particles are transmitted through the barrier, where the spectrum is split into multiple discrete energies. **Lower panel:** when the barrier is narrower, then for specific barrier widths, Fano resonances appear and the particles are totally reflected (with 100% probability).

Using the boundary conditions at $x = 0$:

$$\psi_l(0) = \psi_r(0) \tag{11}$$

$$\psi'_l(0) - \psi'_r(0) = -(\alpha + \beta \cos(\omega t))\psi_r(0) \tag{12}$$

where the tags stand for spatial derivations.

The problem reduces to the following difference equation:

$$-\chi_n \delta(n) = (\alpha - \chi_n) s_n + \frac{\beta}{2} (s_{n+1} + s_{n-1}) \tag{13}$$

where $s_n \equiv t_n(\varphi_n^+ / \varphi_0^+)$,

$$\chi_n \equiv \frac{\varphi_n^{+'}}{\varphi_n^+} - \frac{\varphi_n^{-'}}{\varphi_n^-} = \frac{1}{G_n^+(0)} \equiv -2\rho_n \tanh[\rho_n L - i \arctan(k_n / \rho_n)] \tag{14}$$

$G_n^+(0) \equiv G_{\Omega_n}^+(0)$ is the outgoing Green function of Equation (7) at $x = 0$ and $\rho_n = \sqrt{U - \Omega_n}$.

Finally, the current through the barrier is:

$$j = 2\Re \sum_{n=-\infty}^{\infty} |t_n|^2 |\tau_n|^2 k_n \tag{15}$$

where \Re represents the real part.

The current Equation (15), as a function of the barrier’s width L , is presented in Figure 4 for a given incoming energy Ω .

In Figure 5, the current is presented as a function of the particle’s incoming energy Ω and the barrier’s width L for the same parameters as in Figure 4 (except Ω). The red color represents a high current, while the blue color represents a low current.

As can be seen in Figures 4 and 5, when the incident particle’s energy is lower than the oscillating energy $\Omega < \omega$, multiple solutions of zero current exist, i.e., several Fano resonances appear for different values of L .

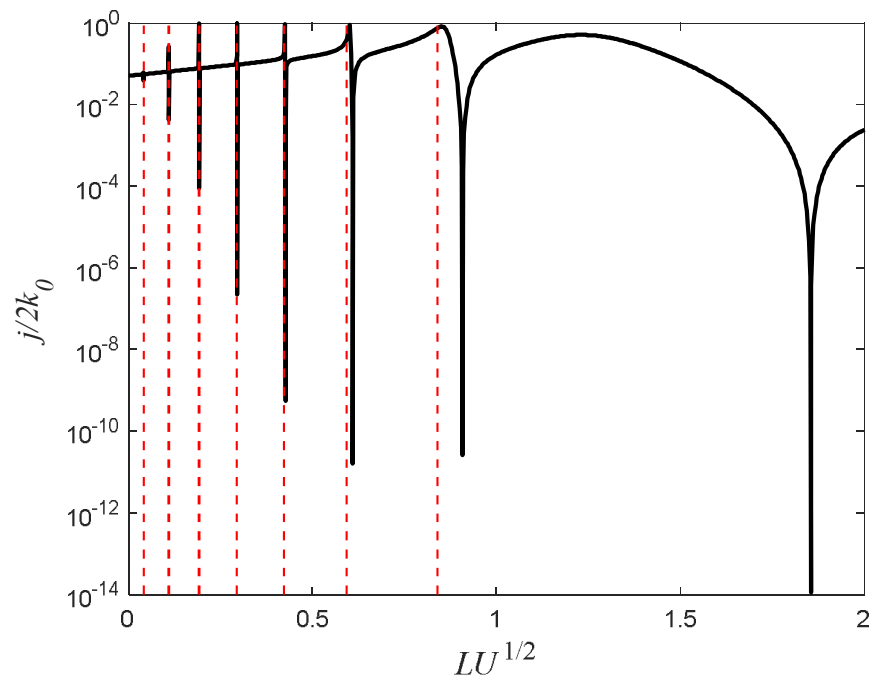


Figure 4. The current (Equation (15)) as a function of the barrier’s width L is presented for $\Omega/U = 0.04$. The vertical red lines represent the analytical solution of Equation (27) for $m = 2, 3 \dots 8$. The other parameters are: $\alpha U^{-1/2} = -1.8$, $\beta U^{-1/2} = 0.4$, and $\omega/U = 0.1$. This simulation is within the regime $\Omega_R < 0$ (Equation (16)).

When the current is presented as a function of both L and Ω , the full structure of these Fano resonances appears. The narrower the barrier, the thinner the Fano resonances, and the lower the oscillation amplitude, the narrower the Fano resonances. Therefore, high-order resonances are very narrow and hard to detect. The zero currents are presented by the multiple curved lines. The zero-current curve (ZCC) on the right, i.e., for $LU^{1/2} \gg 1$, approximately agrees with Equation (5) for $L(\Omega - 3\omega)$. It should be noted that, since during the dynamic process, the instantaneous resonance energy varies in time, the resonance energy (Equation (4)) should be replaced with the minimum resonance energy, i.e.,

$$\Omega_R \cong U - (|\alpha| + \beta)^2/4 \tag{16}$$

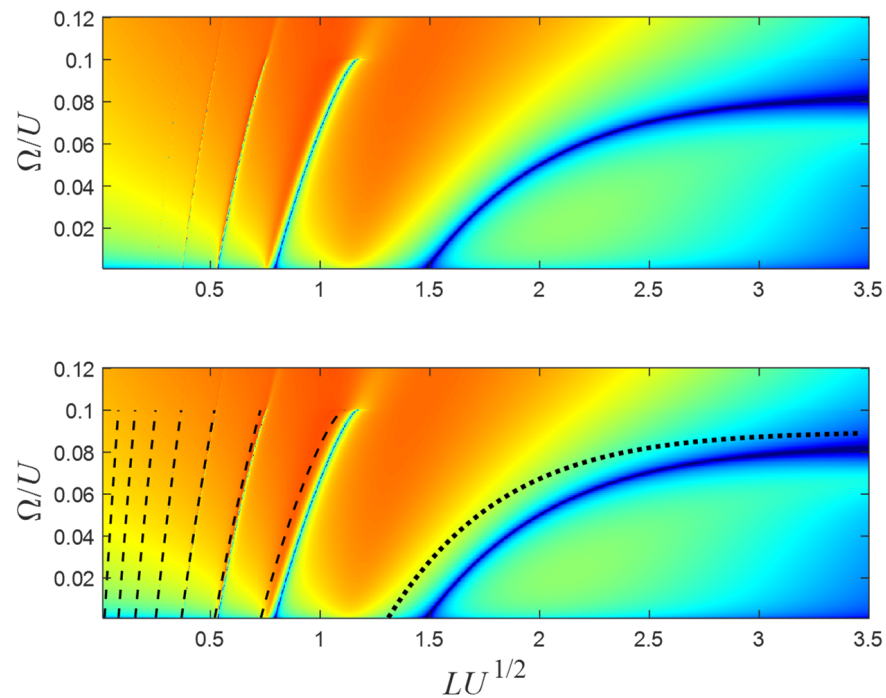


Figure 5. The current (in logarithmic scale) as a function of the particle’s incoming energy Ω and the barrier’s width L . Red color represents high current while blue represents low current. The analytical results are presented on the lower panel. The black dashed curves are the analytical solutions of Equation (27) for $m = 2, 3 \dots 8$, and the dotted black curve is the solution of Equation (17) for $m = 3$ and Ω_R , according to Equation (16). The simulation was based on the same parameters as in Figure 4.

Moreover, the other curves approximately agree with $L(\Omega - m\omega)$ for $m = 3, 4 \dots$. That is, these ZCCs can be regarded approximately as a folded curve. The curves cannot exceed the oscillating frequency $\Omega < \omega$. The number of ZCCs (N) is finite, which can be evaluated by dividing the bare well’s (i.e., without the barrier) depth by the oscillating frequency ω , i.e., $N \cong \alpha^2/4\omega$. In the case presented in Figures 4 and 5, indeed, $N \cong 8$.

Equation (5) can be used to distinguish between two scenarios. There are two regimes in which L has a real value. In the first scenario, the REOB is negative, $\Omega_R < 0$ (Equation (16)), in which case, a real solution exists, provided $\Omega_R - U < \Omega - n\omega < \Omega_R$. In this scenario, the Fano resonance exists even for very opaque barriers, i.e., L can be arbitrarily large. In the second scenario, the REOB is positive, $0 < \Omega_R < U$, in which case, a real solution exists, provided $\Omega_R - U < \Omega - n\omega < 0$. In this scenario, Fano resonance exists only for finite-width barriers. Specifically, L must be narrower than L_0 (Equation (6)).

The second scenario is presented in Figures 6 and 7. It can clearly be shown that, unless the barrier’s width is narrower than a certain cut-off value, no Fano resonances appear. In particular, this scenario does not support a Fano resonance (and hence no zero transmission) in the opaque barrier regime. The discrepancy between the cut-off value of the barrier’s width and L_0 (Equation (6)) is due to the fact that Equation (6) was calculated assuming $\beta = 0$. It will be shown that, when β is weak, there is an excellent agreement with Equation (6).

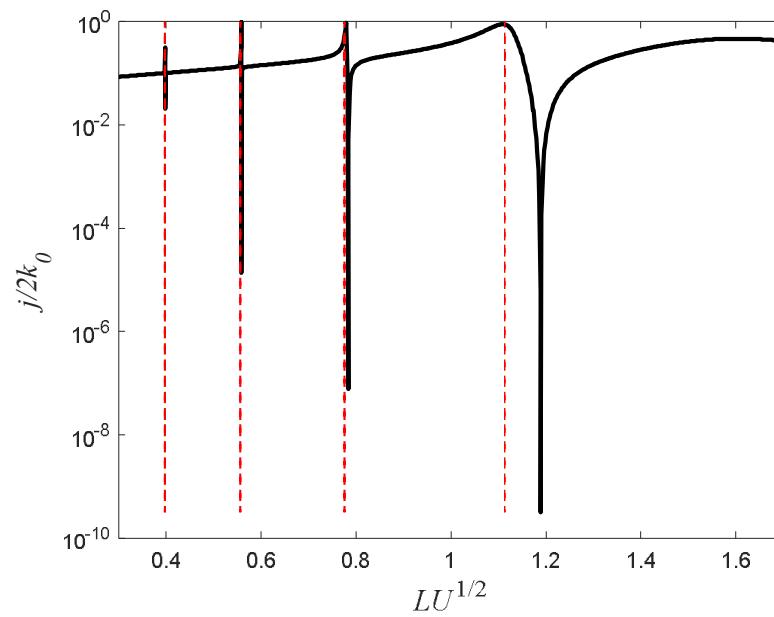


Figure 6. Same as Figure 4 but for the amplitude $\beta U^{-1/2} = 0.19$, i.e., for the second scenario ($0 < \Omega_R < U$). The vertical dashed red lines represent the analytical solution of Equation (27) for $m = 1, 2, 3$, and 4.

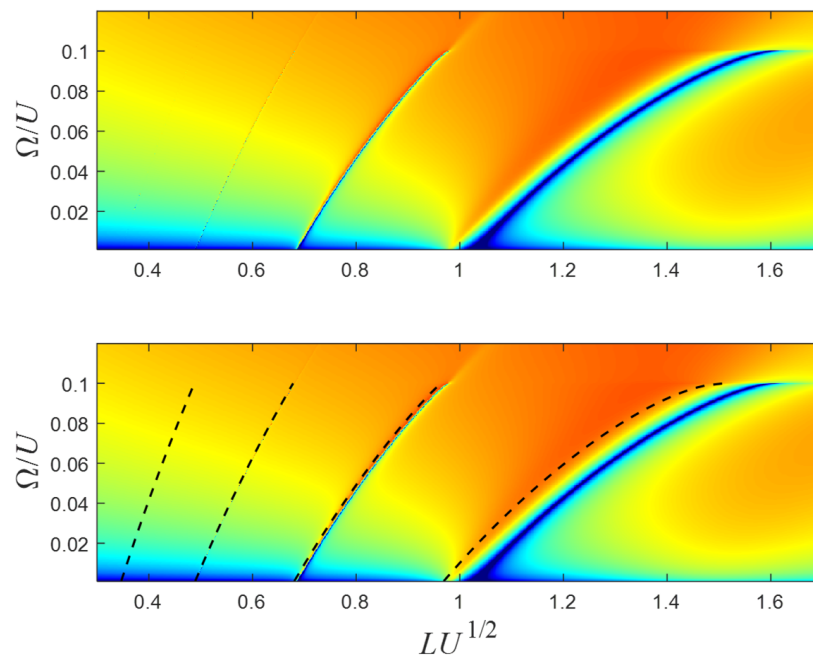


Figure 7. The current as a function of the particle’s incoming energy Ω and the barrier’s width L . The black dashed curves on the lower panel are the analytical solutions of Equation (27). The parameters are as in Figure 6.

The multiple solutions of L_n can be derived qualitatively by replacing Ω with $\Omega - n\omega$ in Equation (5), yielding:

$$L_n \cong \frac{\operatorname{arctanh}\left(\sqrt{\frac{U-\Omega_R}{U-\Omega+n\omega}}\right) - \operatorname{arctanh}\left(\sqrt{\frac{-\Omega+n\omega}{U-\Omega+n\omega}}\right)}{\sqrt{U-\Omega+n\omega}} \tag{17}$$

These solutions are plotted in Figure 8 for $0 < \Omega < \omega$ for two scenarios. It is worth noting the qualitative similarity between the upper/lower panels of Figure 8, and Figure 5/Figure 7, respectively. The folding nature of Equation (17) can be presented by the following relation:

$$L_n(\Omega) = L_0(\Omega - n\omega) \tag{18}$$

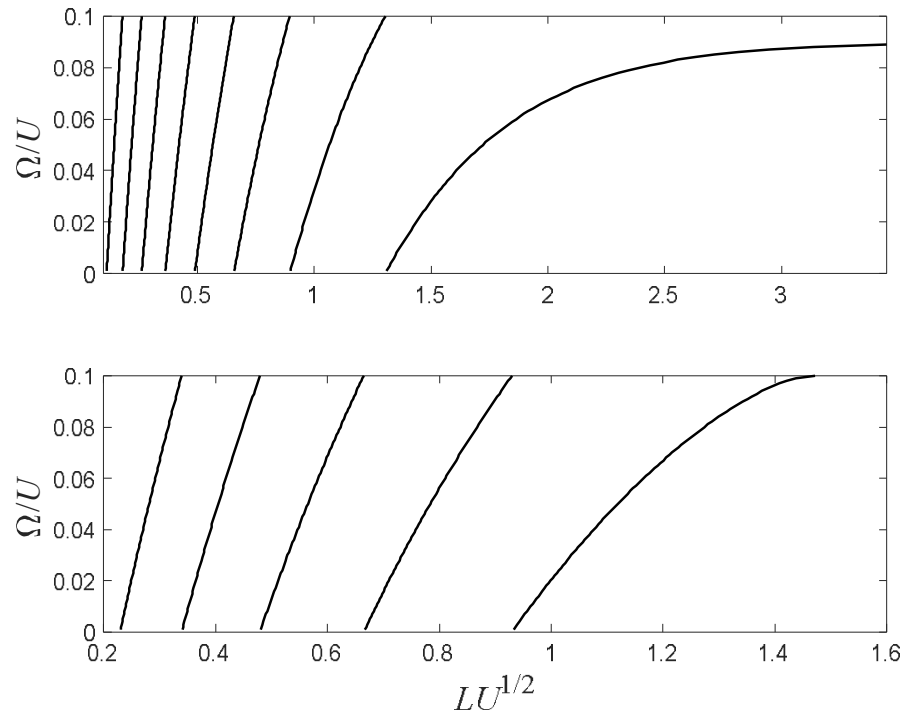


Figure 8. Multiple solutions of Equation (17) for two cases. In the upper panel, Equation (17) is presented for $m = 3, 4 \dots 10$ for the parameter $\alpha U^{-1/2} = -2.2$ ($\Omega_R < 0$). In this scenario, the Fano resonance exists even for very opaque barriers, where L can be arbitrarily large. In the lower panel, Equation (17) is presented for $m = 1, 2 \dots 5$ and for the parameter $\alpha U^{-1/2} = -1.8$ ($\Omega_R > 0$). In this scenario, the Fano resonance exists only for finite-width barriers. In both cases, $0 < \Omega < \omega$ with the parameter $\omega/U = 0.1$.

4. Exact Numerical Solution and Approximate Analytical Solution for the Zero-Transmission Solution

Equation (13) can be rewritten in a matrix form $Mt = v$, where

$$M = \begin{pmatrix} \ddots & & & & & & & & & & \\ & \ddots & & & & & & & & & \\ & & \alpha - \chi_{-2} & & & & & & & & \\ & & \beta/2 & \alpha - \chi_{-1} & & & & & & & \\ & & \beta/2 & \beta/2 & \alpha - \chi_0 & & & & & & \\ & & & \beta/2 & \beta/2 & \alpha - \chi_1 & & & & & \\ & & & & \beta/2 & \beta/2 & \alpha - \chi_2 & & & & \\ & & & & & \beta/2 & \beta/2 & \alpha - \chi_3 & & & \\ & & & & & & \ddots & \ddots & & & \\ & & & & & & & \ddots & \ddots & & \\ & & & & & & & & \ddots & \ddots & \end{pmatrix} \text{ and } v = \begin{pmatrix} \vdots \\ 0 \\ 0 \\ -\chi_0 \\ 0 \\ 0 \\ \vdots \end{pmatrix} \tag{19}$$

and $\chi_n \equiv -2\rho_n \tanh[\rho_n L - i \arctan(k_n/\rho_n)]$ (Equation (14)).

Let us further define

$$M_{(-1)}^{(-N)} = \begin{pmatrix} \alpha - \chi_{-N} & \beta/2 & & & & \\ \beta/2 & \ddots & \ddots & & & \\ & \ddots & & \beta/2 & & \\ & & & \beta/2 & \alpha - \chi_{-2} & \beta/2 \\ & & & & \beta/2 & \alpha - \chi_{-1} \end{pmatrix} \tag{20}$$

and

$$M_{(N)}^{(1)} = \begin{pmatrix} \alpha - \chi_1 & \beta/2 & & & & \\ \beta/2 & \alpha - \chi_2 & \beta/2 & & & \\ & \beta/2 & \ddots & \ddots & & \\ & & \ddots & & \beta/2 & \\ & & & & \beta/2 & \alpha - \chi_N \end{pmatrix} \tag{21}$$

Then, the solution of the zero mode t_0 reads (for details see ref. [34]),

$$t_0 = -\chi_0 \lim_{N \rightarrow \infty} \frac{|M_{(-1)}^{(-N)}| |M_{(N)}^{(1)}|}{|M_0^{(N)}|} \tag{22}$$

Therefore, zero transmission is reached when

$$|M_{(-1)}^{(-N)}| = 0 \tag{23}$$

It follows from Equation (11) and current conservation that, when Equation (22) vanishes, the current must vanish as well. Therefore, the solution of Equation (23) corresponds to the multiple solutions for which the current vanishes.

For any given energy, several solutions exist for different values of L . Nevertheless, we can straightforwardly deduce that Equation (23) is valid, provided that the incoming particle's energy is lower than the oscillating frequency, i.e., $\Omega < \omega$. Otherwise, some of the k_{-m} (for $1 < m < N$) are real, and if this is the case, then the term

$\chi_{-m} = -2\rho_{-m} \tanh[\rho_{-m}L - i \arctan(k_{-m}/\rho_{-m})]$ (Equation (14)) (which are the only elements in the matrix (20) that can have imaginary components) is *not* necessarily real (noting that all the ρ_{-m} terms are real). Consequently, the determinant is not real and cannot vanish. This fact is consistent with the fact that the Fano resonances are limited by $\Omega < \omega$, and with the folding nature of the periodicity, a 2D map structure qualitatively similar to Figure 8 appears.

5. Weak Modulation Regime

In the weak modulation amplitude (β) regime at the vicinity of $\alpha \cong \chi_{-m}$, the determinant of (20) can be written as approximately:

$$|M_{(-1)}^{(-N)}| = (\alpha - \chi_{-m}) |M_{(-m-1)}^{(-N)}| |M_{(-1)}^{(-m+1)}| - \frac{\beta^2}{4} (|M_{(-m-1)}^{(-N)}| |M_{(-1)}^{(-m+2)}| + |M_{(-m-2)}^{(-N)}| |M_{(-1)}^{(-m+1)}|) + O(\beta^4) \tag{24}$$

which can also be rewritten as:

$$|M_{(-1)}^{(-N)}| \cong \prod_{m'=1}^N (\alpha - \chi_{-m'}) \left[1 - \frac{\beta^2}{4} \frac{1}{(\alpha - \chi_{-m})} \left(\frac{1}{(\alpha - \chi_{-m-1})} + \frac{1}{(\alpha - \chi_{-m+1})} \right) + O(\beta^4) \right] \tag{25}$$

Therefore, the transmission vanishes (Equation (23) is valid) up to the second order in β , provided that:

$$1 \cong \frac{\beta^2}{4} \frac{1}{(\alpha - \chi_{-m})} \left(\frac{1}{(\alpha - \chi_{-m-1})} + \frac{1}{(\alpha - \chi_{-m+1})} \right) \tag{26}$$

Since χ_n is a function of L , one can find an expression for the relation between the zero-transmission energy Ω and the width of the barrier L :

$$L_m(\Omega) \cong \frac{\operatorname{arctanh} \left\{ \frac{1}{2\rho_{-m}} \left[\frac{\beta^2}{8i} \left(\frac{1}{(k_{-m}-k_{-m-1})} + \frac{1}{(k_{-m}-k_{-m+1})} \right) - \alpha \right] \right\} + i \operatorname{arctan} \left(\frac{k_{-m}}{\rho_{-m}} \right)}{\rho_{-m}} \tag{27}$$

In the regime where the barrier is opaque, i.e., $LU^{1/2} \gg 1$, Equation (27) can be approximated by:

$$(\alpha + 2\rho_{-1}) \cong \frac{1}{(\alpha + 2\rho_{-2})} \left(\frac{\beta}{2} \right)^2, \text{ and when } \beta \ll \alpha, \text{ it can be solved for the energy:}$$

$$\Omega_c \cong U + \omega - \frac{1}{4} \left[\alpha - \frac{(\beta/2)^2}{\alpha + 2\sqrt{\omega + \alpha^2/4}} \right]^2 \tag{28}$$

Expression (27) is presented in Figures 4–7. The discrepancy between this expression and the numerical results, which is larger for low orders, is due to the fact that Equation (27) is derived for a weak β . In the following Figures 9–12, since β is smaller, there is a better agreement with Equation (27).

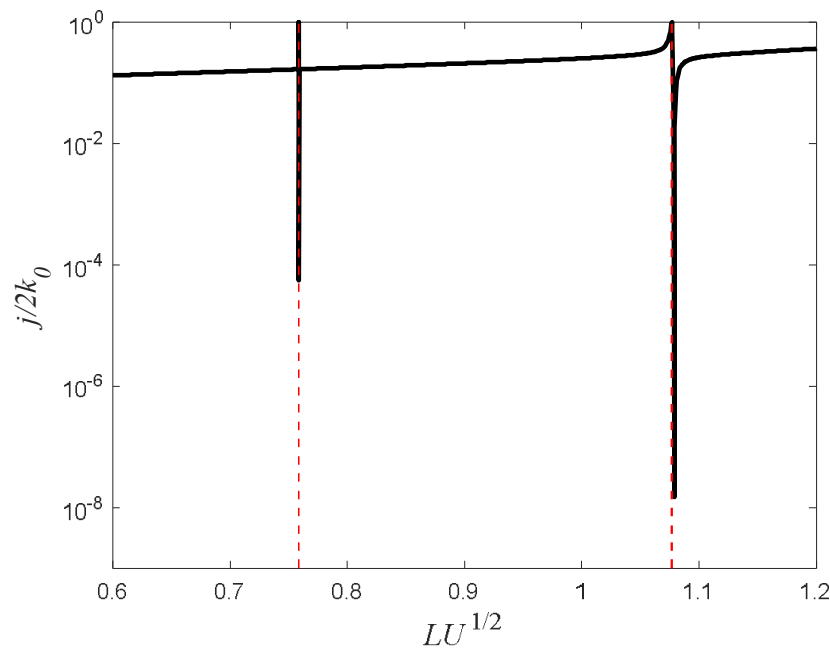


Figure 9. The current as a function of the barrier’s width L for $\Omega/U = 0.04$ in the second scenario regime ($0 < \Omega_R < U$). The dashed red vertical lines are the solutions for zero transmission (Equation (27) for $m = 1, 2$). The other parameters are: $\alpha U^{-1/2} = -1.8$, $\beta U^{-1/2} = 0.03$, and $\omega/U = 0.1$.

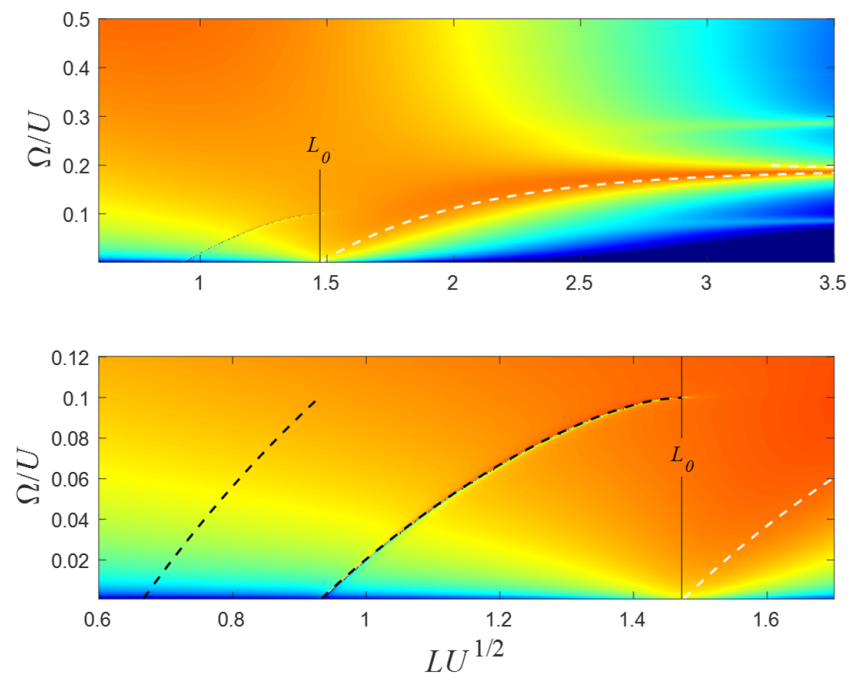


Figure 10. The current as a function of the particle’s incoming energy Ω and the barrier’s width L in the second scenario regime ($0 < \Omega_R < U$). The lower panel is an enlargement of the upper one. The white dashed curve is the solution of Equation (5), where L_0 is Equation (6). The dashed black curves are the solution for zero transmission (Equation (27)). The parameters are the same as in Figure 9.

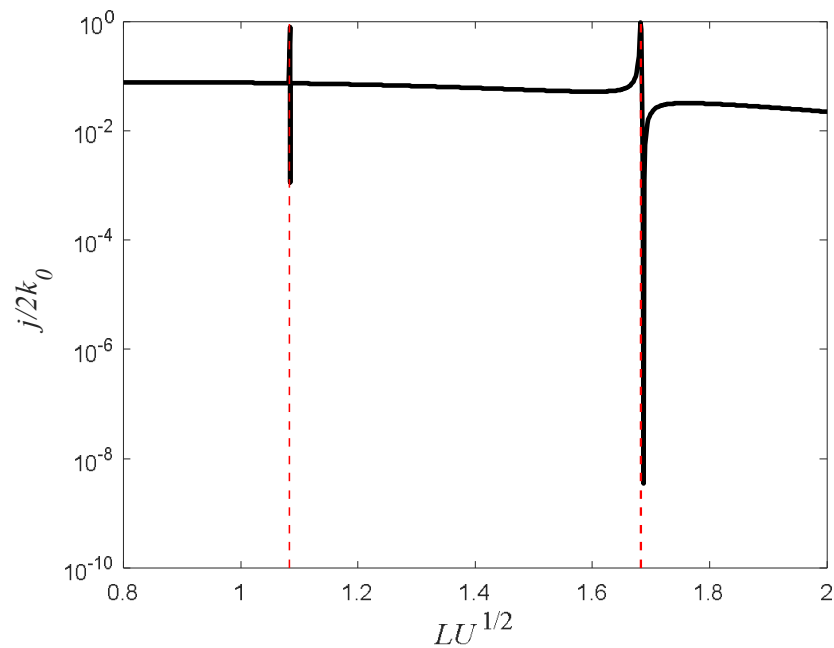


Figure 11. The current as a function of the barrier’s width L is presented for $\Omega/U = 0.04$. The vertical dashed red lines represent the analytical solution of Equation (27) for $m = 2, 3$. The other parameters are: $\alpha U^{-1/2} = -2.1$, $\beta U^{-1/2} = 0.08$, and $\omega/U = 0.1$, i.e., $\Omega_R < 0$.

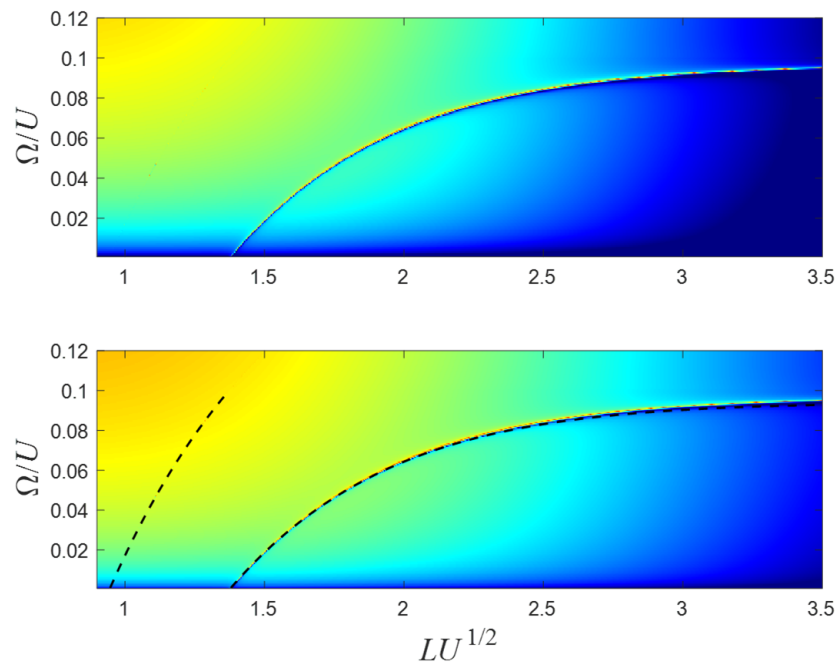


Figure 12. The current as a function of the particle’s incoming energy Ω and the barrier’s width L . The black dashed curves on the lower panel are the analytical solutions of Equation (27) for $m = 2, 3$. These are the same parameters as in Figure 11.

In Figures 9 and 10, the second scenario (i.e., $0 < \Omega_R < U$) is presented for a weak β . In Figures 11 and 12, the first scenario (i.e., $\Omega_R < 0$) is presented for a weak β . As can be seen in both cases, the agreement with the theoretical prediction (Equation (27)) is excellent.

6. Narrow Barrier Regime

In the narrow barrier regime, i.e., when the width of the barrier is considerably narrower than the incoming particle’s wavelength, Equation (26) can be rewritten as:

$$1 \cong \frac{\beta^2}{4} \frac{1}{(\alpha_0 - \chi_{-m})} \left(\frac{1}{(\alpha_0 - \chi_{-m-1})} + \frac{1}{(\alpha_0 - \chi_{-m+1})} \right) \tag{29}$$

where $\alpha_0 = \alpha + UL$. In which case, $\Omega \cong m\omega - \frac{\alpha_0^2}{4} - \frac{\beta^2}{8}$, or equivalently:

$$\Omega \cong m\omega - \frac{(\alpha + UL_m)^2}{4} - \frac{\beta^2}{8} \tag{30}$$

This expression relates the different barrier widths L_m , which yield Fano resonances, to the same energy Ω . In what follows, we will investigate the implications of this.

7. Strong Oscillations and Opaque Barrier Regime

In the wide barrier regime, i.e., when the barrier is opaque, the dependence of the resonance energy on the barrier’s width L is exponentially small and can therefore be neglected. Furthermore, in this regime, the particle is approximately trapped in the well and the QBSS is well defined. It has been shown that the transmission via this state is extremely sensitive to the incoming particle’s energy (Ω). For some values of Ω , which are consistent with the spectral component of the QBSS, the QBSS is highly excited and, consequently, the tunneling current is very high. Similarly, for other energy values, which are inconsistent with the spectral components of the QBSS, the particle cannot be trapped and the tunneling

current is highly suppressed. These scenarios have been well investigated [10,14,18]. In particular, it has been found that current suppression occurs for the energies:

$$\int_{t_1}^{t_2} (\Omega - \Omega_R(t')) dt' = \left(m - \frac{1}{4}\right)\pi \tag{31}$$

where, for the case under study, i.e., Equation (7),

$$\Omega_R(t) = U - \frac{(\alpha + \beta \cos(\omega t))^2}{4} \tag{32}$$

is the instantaneous resonance energy of the well and t_1 and t_2 are the solutions of $\Omega = \Omega_R(t)$ [10,14,18], i.e., these are the instances in which the incoming particle's energy coincides with the instantaneous resonant state's energy. The solutions of (31) for the case (32) are:

$$\Omega_m \cong U - \left(\frac{\alpha^2}{4} + \frac{\beta^2}{8}\right) - \left[\frac{|\alpha|\beta}{\pi} - 2\omega\left(m - \frac{1}{4}\right)\right] \tag{33}$$

Similarly, for a given incoming energy, the oscillating amplitudes, which correspond to the current suppression, are:

$$\beta_m = -\frac{4|\alpha|}{\pi} + \sqrt{\frac{16\alpha^2}{\pi^2} + 8\left(U - \Omega - \frac{\alpha^2}{4} + 2\omega\left(m - \frac{1}{4}\right)\right)} \tag{34}$$

However, although this expression has been found to be in good agreement with numerical simulations, it only predicts current suppression. It does not predict zero current. The reason for this is that, as has been explained in refs. [10,11], at the suppression energies, only the upper half of the spectrum ($\Omega_{out} \geq \Omega_{in}$) is suppressed. Therefore, in a case where the incoming energy is higher than the oscillating frequency $\Omega > \omega$, the lower part of the spectrum still includes propagating modes, since the particle can lose a quantum ω and still escape from the well. To prevent this, the existence of a Fano resonance (and zero transmission) requires the additional condition (additional to (31)) that $\Omega < \omega$, in which case, the output spectrum consists of only negative energies. Therefore, positive energies cannot propagate and the incoming particles are completely reflected. This required additional condition is consistent with the explanation that follows Equation (23). The difference between these two kinds of suppressions (low current vs. zero current) is illustrated in Figure 13, where the current, as a function of the incoming energy Ω and a function of the oscillation amplitude β , is presented. When the incoming energies are lower than the oscillation frequency $\Omega < \omega$, a total reflection appears for appropriate amplitudes. In the lower panel, the analytical results of Equation (33) are presented by dashed black curves above the numerical results. The analytical results represent suppression scenarios; however, the suppressions' characteristics are fundamentally different in the regions $\Omega < \omega$ and $\Omega > \omega$. In the region $\Omega < \omega$, the suppression manifests in 100% reflection, whereas in the region $\Omega > \omega$, the current suppression is substantial, albeit not entirely zero.

Figure 14 illustrates the difference between the two regimes. The current is plotted as a function of the oscillation amplitudes for two adjacent incoming energies. One of the energies is slightly lower than the oscillation frequency ω and the other is slightly higher than the oscillation frequency. Although the two plots look alike, they are fundamentally different. When $\Omega/\omega = 0.99$, the minima are exactly zero, while, when $\Omega/\omega = 1.01$, the suppression is indeed substantial, but does not go to zero. Moreover, as can be seen with the vertical red lines, the analytical expression of the suppression amplitude β_m (Equation (34)) agrees with the numerical results.

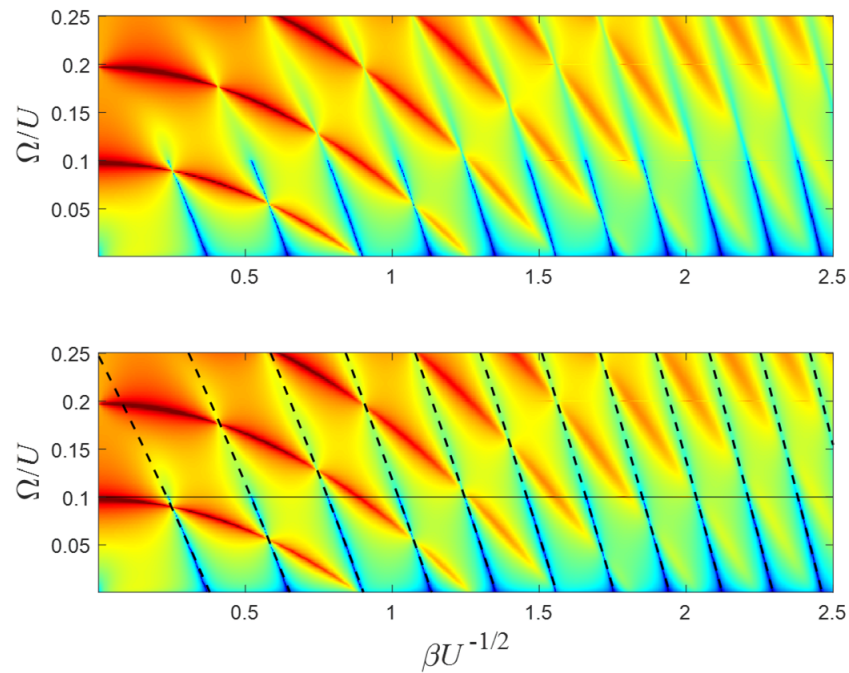


Figure 13. The current as a function of the incoming energy and the oscillation amplitudes. On the lower panel, the black dashed curves represent the analytical expressions (Equation (33)) and the horizontal line represents the $\Omega = \omega$ boundary. The parameters are $LU^{1/2} = 5$, $\alpha U^{-1/2} = -1.9$ and $\omega/U = 0.1$.

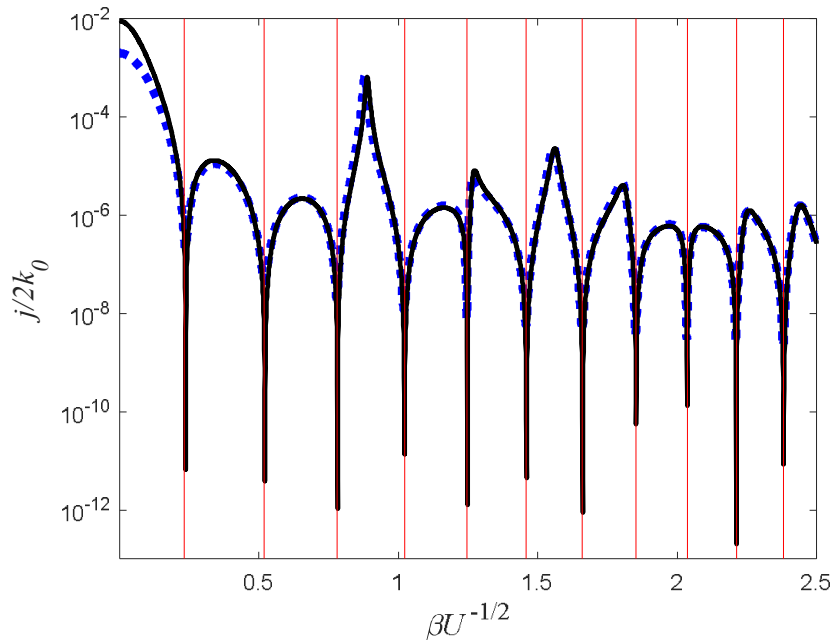


Figure 14. Comparison between the two types of suppressions: the current as a function of the oscillation amplitude is presented for two adjacent incoming energies, $\Omega/\omega = 1.01$ with a thick blue dotted curve and $\Omega/\omega = 0.99$ with a black curve. The vertical red lines are the solution of β_m (Equation (34)) for $m = 1, 2, \dots, 12$. These are the same parameters as in Figure 13.

8. High Precision Interferometry

When an object is measured with a wave beam, then usually, the shorter the wavelength, the better the resolution. In the case of a simple rectangular barrier, the interference between the reflections from its boundaries determines the dynamic range of the measure-

ment. Therefore, if a small object with dimensions $\sim \Delta L$ is measured, then, unless the particle's frequency is of the order $\sim \Delta L^{-2}$, the dynamic range would be minuscule and of the order of $(\Delta L/\lambda)^2 \ll 1$, where λ is the particle's de-Broglie wavelength.

Ref. [18] suggested fabricating a quantum device like the one presented in Equation (7) and Figure 3 as a frequency-controlled quantum transistor. The oscillations can be confined in space using well-known technology (see, for example, ref. [35]). The present work teaches that the dynamic range of these devices can be increased substantially.

The Fano nature of these resonances shows that the dynamic range is almost 100%, regardless of the barrier's width and oscillating frequency.

In the case where the oscillating part (width ε and height V) and measured object (width L and height U) are very narrow in comparison to the incoming particle's wavelength, Equation (30) can be simplified to (since now $\alpha_0 \cong V\varepsilon$):

$$\Omega \cong m\omega - \frac{(V\varepsilon + UL_m)^2}{4} - \frac{\beta^2}{8} \tag{35}$$

This equation can be rewritten as:

$$\Omega \cong \left[-\frac{(V\varepsilon + UL_m)^2}{4} - \frac{\beta^2}{8} \right] \text{mod}\omega \tag{36}$$

where mod represents the modulo operation.

In the case where $\alpha_0 \gg UL_m$, then the widths L_m , for which zero transmission is reached, must maintain:

$$\Omega \cong m\omega - \frac{\alpha_0^2 + 2\alpha_0UL_m}{4} - \frac{\beta^2}{8} \tag{37}$$

Therefore, the difference between the adjacent widths is $L_m - L_{m+1} = \Delta L \cong \frac{2\omega}{\alpha_0 U}$. Or, equivalently, a change δL in the barrier's width will change the zero-transmission energy by:

$$\Delta\Omega \cong \frac{V\varepsilon U}{2} \delta L \tag{38}$$

In real physical units, Equation (38) can be written as $\Delta\Omega \cong \frac{m}{\hbar^3} VU\varepsilon\delta L$, where m represents the effective mass in the material, which, for GaAs (where the effective mass is 0.067 times the mass of the free electron [35]), Equation (38) can therefore be written as:

$$\Delta\Omega[\text{Hz}] \cong 1.5 \times 10^{15} VU\varepsilon\delta L \tag{39}$$

In Equation (39), the potential heights V and U are measured in eV and their widths ε and δL are measured in nanometers. The change in the frequency is measured in Hz.

Therefore, if the oscillating part and measured object have a potential of ~ 0.01 eV and a width of ~ 1 nm, then every change of 0.01 nm (0.1 \AA) varies the zero-transmission frequency by more than 1.5 GHz. Clearly, this result is valid, provided that the oscillating frequency is higher than this value. These values are easily achievable using contemporary electronics. Since the frequency can be measured with great accuracy, this device can exhibit an extremely high precision. Furthermore, unlike ordinary measurements, as was described at the beginning of this section, where high energy is required to achieve a high precision, such a requirement is not necessary and does not limit the performance of this device, which can operate in low energies.

Furthermore, since the measurement is taken where the current is zero, this device is highly resilient against different kinds of noises, especially shot noise, which should vanish at these points, thus having a negligible effect on the measurement. The presence of thermal noise (which can be reduced by lowering the temperature) would require more extended measurement periods (for averaging), in which case, a minimum current should be sought instead of a zero current, but Equation (39) should still be valid.

Such a device can be applied in several configurations. It can be used as a highly sensitive frequency-controlled transistor, where minuscule variations in the frequency can change the current drastically, or alternatively, it can be used as a high-precision measurement device for measuring nanostructures' dimensions with sub-nanometer precision.

9. Conclusions and Summary

The tunneling current through a barrier via an oscillating well was investigated both numerically and analytically. While previous works have focused on the difference between high transmission (activation) and low transmission (current suppression), this work focused on the difference between current suppression and zero transmission. Since zero transmission is equivalent to a Fano resonance, it requires interference with a bound state. The following are the main conclusions:

- (A) A bound state can exist even when the well's bound state is smaller (in absolute terms) than the height of the barrier ($\alpha^2/4 < U$), and an analytical expression was derived to relate the resonance state to the barrier's width $L(\Omega_R)$. It was shown that the resonance state decreases when the barrier's width shrinks. Therefore, if the barrier is narrow enough, the resonance state would eventually turn into a bound state.
- (B) When an oscillating term is introduced, it was shown that zero transmission (and therefore zero current) requires the incoming particle's energy to be lower than the oscillating energy, i.e., $\Omega < \omega$.
- (C) Since the particle can gain/lose oscillating quanta, for any given incoming energy, multiple solutions of the barrier's width exist, and from (A) and (B), it follows that the solution curve is folded. Therefore, the solutions can be retrieved qualitatively: $L_n(\Omega) = L_0(\Omega - n\omega)$.
- (D) It was found that there are two different scenarios:
 - (1) When the Resonance Energy of the Opaque Barrier (REOB) is negative. In this scenario, the Fano resonance (zero transmission) occurs even for an infinitely wide barrier.
 - (2) When the REOB is positive, the barrier must be narrower than a certain value for a Fano resonance to appear.
- (E) An analytical expression was derived for the barrier's width, which supports Fano resonances $L_m(\Omega)$ up to the second order in the oscillation amplitude β^2 , and it was found to be in high agreement with exact numerical results.
- (F) In the case where the oscillation amplitude is large, one can use the method that was applied to the Sisyphus effect and the QBSS method [14,17], along with the additional requirement of $\Omega < \omega$, calculating the Fano criteria with a high agreement with numerical simulations.
- (G) Finally, it was shown that, in the case of a very narrow barrier, a simple analytical expression relates the zero-transmission energy to the multiple barrier widths $L_n(\Omega)$, which support the Fano resonance. This expression shows that the energy, which can easily be measured, is extremely sensitive to the barrier's width, and can therefore be used for high-precision measurements.

Author Contributions: Conceptualization, G.Z. and E.G., methodology, G.Z. and E.G., software, G.Z. and E.G., formal analysis, G.Z. and E.G., investigation, G.Z. and E.G., writing, G.Z. and E.G. All authors have read and agreed to the published version of the manuscript.

Funding: This research received no external funding.

Institutional Review Board Statement: Not applicable.

Informed Consent Statement: Not applicable.

Data Availability Statement: Not applicable.

Conflicts of Interest: The authors declare no conflict of interest.

References

1. Chynoweth, A.G.; Logan, R.A.; Thomas, D.E. Phonon-assisted tunneling in silicon and germanium Esaki junctions. *Phys. Rev.* **1962**, *125*, 877. [[CrossRef](#)]
2. Fujisawa, T.; Tarucha, S. Photon assisted tunneling in single and coupled quantum dot systems. *Superlatt. Microstruct.* **1997**, *21*, 247. [[CrossRef](#)]
3. Shchurova, L.Y.; Murzin, V.N. Phonon-Assisted Tunneling Current in a Double-Barrier Heterostructure with a Quantum Well. *J. Russ. Laser Res.* **2021**, *42*, 632–642. [[CrossRef](#)]
4. Vdovin, E.E.; Mishchenko, A.; Greenaway, M.T.; Zhu, M.J.; Ghazaryan, D.; Misra, A.; Cao, Y.; Morozov, S.V.; Makarovskiy, O.; Fromhold, A.; et al. Phonon-assisted resonant tunneling of electrons in graphene boron nitride transistors. *Phys. Rev. Lett.* **2016**, *116*, 186603. [[CrossRef](#)] [[PubMed](#)]
5. Kot, P.; Drost, R.; Uhl, M.; Ankerhold, J.; Cuevas, J.C.; Ast, C.R. Microwave-assisted tunneling and interference effects in superconducting junctions under fast driving signals. *Phys. Rev. B* **2020**, *101*, 134507. [[CrossRef](#)]
6. Platero, G.; Aguado, R. Photon-assisted transport in semiconductor nanostructures. *Phys. Rep.* **2004**, *395*, 1–157. [[CrossRef](#)]
7. Kohler, S.; Lehmann, J.; Hänggi, P. Driven quantum transport on the nanoscale. *Phys. Rep.* **2005**, *406*, 379. [[CrossRef](#)]
8. Azbel, M.Y. Elevator resonance activation. *Europhys. Lett.* **1992**, *18*, 537. [[CrossRef](#)]
9. Azbel, M.Y. Eigenstate Assisted Activation. *Phys. Rev. Lett.* **1992**, *68*, 98. [[CrossRef](#)]
10. Zangwill, G.; Granot, E. Eigenstate suppressed activation. *Physica B* **2015**, *461*, 140. [[CrossRef](#)]
11. Granot, E. Selected elevation in quantum tunneling. *Europhys. Lett.* **2003**, *61*, 817. [[CrossRef](#)]
12. Wagner, M. Quenching of resonant transmission through an oscillating quantum well. *Phys. Rev. B* **1994**, *49*, 16544. [[CrossRef](#)] [[PubMed](#)]
13. Wagner, M. Photon-assisted transmission through an oscillating quantum well: A transfer-matrix approach to coherent destruction of tunneling. *Phys. Rev. A* **1995**, *51*, 798. [[CrossRef](#)]
14. Zangwill, G.; Granot, E. Dynamic resonant tunneling via a quasibound superstate. *Phys. Rev. A* **2022**, *106*, 032201. [[CrossRef](#)]
15. Zangwill, G.; Granot, E. Spatial vibrations suppressing resonant tunneling. *Phys. Rev. A* **2020**, *101*, 012109. [[CrossRef](#)]
16. Lauhon, L.J.; Ho, W. Direct Observation of the Quantum Tunneling of Single Hydrogen Atoms with a Scanning Tunneling Microscope. *Phys. Rev. Lett.* **2000**, *85*, 4566. [[CrossRef](#)]
17. Granot, E. The tunneling current through oscillating resonance and the Sisyphus effect. *Adv. Condens. Matter Phys.* **2017**, *2017*, 2435857. [[CrossRef](#)]
18. Granot, E.; Zangwill, G. Dynamic resonant tunneling. In *Quantum Dynamics*; Bracken, P., Ed.; InTech: Rijeka, Croatia, 2016; p. 55.
19. Grifoni, M.; Hänggi, P. Driven quantum tunneling. *Phys. Rep.* **1998**, *304*, 229. [[CrossRef](#)]
20. Ben-Asher, A.; Šimsa, D.; Uhlí, T.; Šindelka, M.; Moiseyev, N. Laser Control of Resonance Tunneling Via an Exceptional Point. *Phys. Rev. Lett.* **2020**, *124*, 253202. [[CrossRef](#)] [[PubMed](#)]
21. Biswas, R.; Sinha, C. Quenching effect of oscillating potential on anisotropic resonant transmission through a phosphorene electrostatic barrier. *Sci. Rep.* **2021**, *11*, 2881. [[CrossRef](#)] [[PubMed](#)]
22. Bagwell, P.F.; Lake, R.K. Resonances in transmission through an oscillating barrier. *Phys. Rev. B* **1992**, *46*, 15329. [[CrossRef](#)]
23. Tekman, E.; Bagwell, P. Fano resonances in quasi-one-dimensional electron waveguides. *Phys. Rev. B* **1993**, *48*, 2553. [[CrossRef](#)]
24. Ueda, A.; Eto, M. Resonant tunneling and Fano resonance in quantum dots with electron-phonon interaction. *Phys. Rev. B* **2006**, *73*, 235353. [[CrossRef](#)]
25. Miroshnichenko, A.E.; Flach, S.; Kivshar, Y.S. Fano resonances in nanoscale structures. *Rev. Mod. Phys.* **2010**, *82*, 2257. [[CrossRef](#)]
26. Thuberg, D.; Reyes, S.A.; Eggert, S. Quantum resonance catastrophe for conductance through a periodically driven barrier. *Phys. Rev. B* **2016**, *93*, 180301(R). [[CrossRef](#)]
27. Briones-Torres, J.A.; Rodriguez-Vargas, I. Fano resonances in bilayer graphene superlattices. *Sci. Rep.* **2017**, *7*, 16708. [[CrossRef](#)] [[PubMed](#)]
28. Cocklin, S.; Morr, D.K. Scanning tunneling shot noise spectroscopy in Kondo systems. *Phys. Rev. B* **2019**, *100*, 125146. [[CrossRef](#)]
29. Razavy, M. *Quantum Theory of Tunneling*; World Scientific: Singapore, 2003.
30. Bohm, D. *Quantum Theory*; Dover Publication: New York, NY, USA, 1989.
31. Chang, L.L.; Esaki, L.; Tsu, R. Resonant tunneling in semiconductor double barriers. *Appl. Phys. Lett.* **1974**, *24*, 593. [[CrossRef](#)]
32. Landau, L.D.; Lifschitz, E.M. *Quantum Mechanics*; Section 46; Pergamon: Oxford, UK, 1976.
33. Merzbacher, E. *Quantum Mechanics*; Wiley: New York, NY, USA, 1970.
34. Granot, E. Derivation of analytical expressions for anomalous reflection in the limit of zero thickness and weakly modulated dielectric grating. *J. Opt. Soc. Am. A* **2022**, *39*, 2205–2213. [[CrossRef](#)]
35. Beenakker, C.W.J.; van Houten, H.; Physics, S.S. *Semiconductor Heterostructures and Nanostructures*; Ehrenreich, H., Turnbull, D., Eds.; Academic Press: San Diego, CA, USA, 1991.

Disclaimer/Publisher's Note: The statements, opinions and data contained in all publications are solely those of the individual author(s) and contributor(s) and not of MDPI and/or the editor(s). MDPI and/or the editor(s) disclaim responsibility for any injury to people or property resulting from any ideas, methods, instructions or products referred to in the content.